SAND2016-10725J

Laser Direct Write Synthesis of Lead Halide Perovskites

Stanley S. Chou[†,*], Brian S. Swartzentruber[‡], Matthew T. Janish[§], Kristin C. Meyer[ǁ], Laura B. Biedermann[†], Serdal Okur[⊥], D. Bruce Burckel[†], C. Barry Carter[‡,§] and Bryan Kaehr[ǁ,#,*]

[†]Sandia National Laboratories, Albuquerque, NM 87185, United States, United States; [‡]Center for Integrated Nanotechnologies, Sandia National Laboratories, Albuquerque, NM 87545, United States; [§]Department of Materials Science & Engineering, University of Connecticut, CT 06269, United States; [ǁ]Advanced Materials Laboratory, Sandia National Laboratories, Albuquerque, New Mexico 87106, United States; [⊥]Department of Electrical and Computer Engineering, the University of New Mexico, Albuquerque, New Mexico 87131, United States; [#]Department of Chemical and Biological Engineering, the University of New Mexico, Albuquerque, New Mexico 87131, United States

[*]correspondence to: schou@sandia.gov; bjkaehr@sandia.gov

Abstract

Lead halide perovskites are increasingly considered for applications beyond photovoltaics, for example, light emission and detection, where an ability to pattern and prototype microscale geometries can facilitate the incorporation of this class of materials into devices. Here we demonstrate laser direct write of lead halide perovskites, a remarkably simple procedure that takes advantage of the inverse dependence between perovskite solubility and temperature by using a laser to induce localized heating of an absorbing substrate. We demonstrate arbitrary pattern formation of crystalline $CH_3NH_3PbBr_3$ on a range of substrates and fabricate and characterize a microscale photodetector using this approach. This direct write methodology provides a path forward for the prototyping and production of perovskite-based devices.

Table of Contents Image

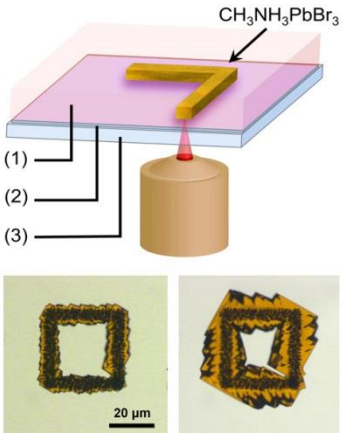

The recent incorporation of lead halide perovskites in photovoltaics (PV) has proven to be a watershed moment for solar energy research and semiconductor materials science. Since the incorporation of methylammonium lead halide ($CH_3NH_3PbX_3$ where X = halide) into solar cells in 2009[1], power conversion efficiency of perovskite-based PV has grown sevenfold—an unprecedented rate of development for solar energy materials. Yet, while the photovoltaic aspect is relatively new, $CH_3NH_3PbX_3$ itself has been explored since the 1970s[2], and the resurgence of this class of materials promises applications beyond PV. Indeed, with long carrier diffusion lengths, defect tolerance and high photoluminescent yield, halide perovskites are being evaluated for light emission,[3] radiography,[4-5] and lasing,[6] among other applications. With the potential to be employed as exceptional semiconductors, there is an anticipation of integrating these materials with traditional (e.g., integrated circuits) and emergent (e.g., flexible electronics) technologies, and thus there is an increasing need to develop methodologies to pattern halide perovskites.

Perovskite patterning appears to have been first reported in 2003 by Cheng *et al.*[7] using a soft lithographic, contact molding approach. More recent work has investigated both lithographic and contact printing methods to pattern perovskite materials. Photolithographic patterning of PbX_2 seeds followed by vapor-phase conversion to perovskites has been shown to achieve uniform, wafer-scale patterning[8-9]; recently Feng *et al.* developed a liquid-contact printing method to control size and location of perovskite crystals[6]. These routes offer potential pathways to scalable patterning, but are inherently multi-step and require the generation of masks and masters to develop new patterns. Thus, there are opportunities to develop complementary processing techniques for perovskites that are more conducive to rapid prototyping and device functionalization including methods that provide for direct-write printing.

To these ends, we set out to develop a direct-write procedure for lead halide perovskites. It was recently demonstrated that lead perovskite precursors exhibit an inverse relationship between solubility and temperature[10]. This relationship provides a simple mechanism to spatially confine crystal growth, e.g., using a laser to induce microscale heating of a transducing substrate. Indeed, this premise turns out to be remarkably straightforward, and allows for the development of laser direct-write (LDW) of lead halide perovskites materials routinely from bath solution. This technique provides site-specific integration of perovskite functionality onto platforms used in electronics as demonstrated here via fabrication of a micro-scale photodetector incorporating a perovskite wire.

As a starting point, we pattern platinum metal crosses onto a glass coverslip using a laser-printing approach[11] to be used as heating pads. This patterned substrate is subsequently bathed in a perovskite precursor solution, such as a stoichiometric ratio of CH_3NH_3Br and $PbBr_2$ dissolved in dimethylformamide (DMF). Next, a wavelength tunable continuous-wave (CW) laser (Titanium:Sapphire; Ti:S) centered at 750 nm (at this wavelength the glass is nearly transparent and Pt absorbs ~ 30% of the light) is focused on the Pt cross to induce heating of the metal to produce a solution temperature sufficient to locally crystalize $CH_3NH_3PbBr_3$ perovskites centered at the metal cross (**Figure 1a-1c, see** *Experimental Methods* for details). Scanning electron microscopy (SEM) images of crystals grown on Pt crosses shown interconnected cuboid crystals >50 μm tall (**Figure S1**). Though both CW and pulsed laser light were sufficient to induce crystallization at this wavelength, ejection of the nascent crystals from the heating pad was more often observed using a pulsed source, likely due to the rapid thermal expansion/compression of the transducer generated under pulsed conditions (60 fs pulse width 80 MHz repetition rate). Consequently, CW mode was preferable for subsequent experiments.

As indicated by transmission electron microscopy (TEM; **Figure 1d**) and powder X-ray diffraction (XRD; **Figure S2**), resultant $CH_3NH_3PbBr_3$ are highly crystalline and of appropriate structure. Briefly, from the TEM Select Area Diffraction (SAD) of the LDW $CH_3NH_3PbBr_3$ crystal (Figure 1d), we measured d = 5.95 Å for (100) and 5.91 Å for (010), which corresponds to the room temperature cubic phase first reported by Poglitsch *et al.*[12] Structural parameters were further confirmed using XRD (Figure S1), which identified similar a = b = c values of 5.83 Å, with space group of *Pm3m*. Though we focus our studies here on the bromides (good stability and potential for applications[13]); importantly, this general procedure is compatible with iodide and chloride methylammonium lead perovskites (**Figure S3**).

Next, we optimized crystal growth parameters through the systematic variation of the concentrations of precursors in solution. For this, perovskite precursors were dissolved in stoichiometric ratios of $PbBr_2$ and CH_3NH_3Br. To fabricate $CH_3NH_3PbBr_3$ crystals, we prepared 1.7 M solutions (≈ solubility limit) in DMF yielding a clear solution.

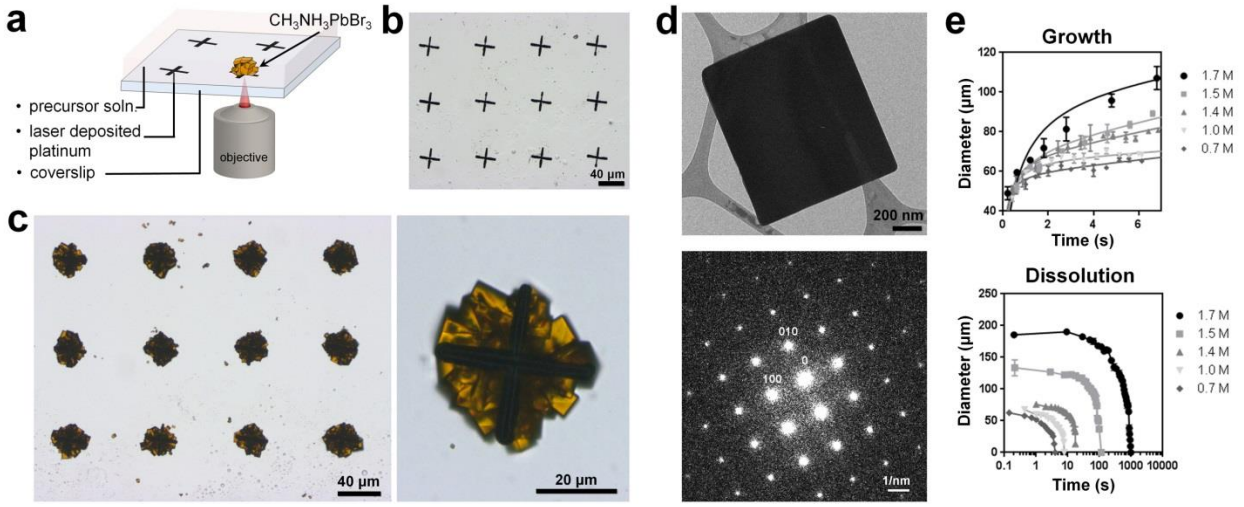

Figure 1. (a) Schematic of the experiment. Platinum crosses are patterned onto glass and immersed in precursor solution. The backside of the Pt metal is heated to induce crystallization of $CH_3NH_3PbBr_3$ perovskite. (b) Laser patterned platinum crosses. (c) An array of $CH_3NH_3PbBr_3$ crystals following laser heating. (d) TEM bright-field image and electron diffraction pattern of a

LDW micro-crystallite with the beam parallel to [100]. (e) Crystal growth and dissolution rates versus precursor concentration for $CH_3NH_3PbBr_3$. Concentrations are 1.7 M, 1.5 M, 1.3 M, 1.0 M and 0.7 M.

Figure 1e shows the relationship between crystal growth, size, and dissolution with precursor concentration. For $CH_3NH_3PbBr_3$, at precursor concentrations from 0.7 M to 1.7 M, we observe stable crystal diameters, defined as the time-point of limited further crystal growth (t = 7 s), to be variable from 60 to 105 μm. Additionally, we observe size dependent dissolution rates of crystals following cessation of laser illumination. As seen in Figure 1e, the persistence time of the crystals is dependent upon the bath concentration of precursors. For concentrations above 1.5 M, dissolution is sufficiently slow, providing an opportunity for extended patterning.

To test this directed pattern possibility, we sputtered a semi-transparent thin film (either Au, C) onto a microscope coverglass. This light-absorbing layer functioned as a transducer to generate localized heating using a configuration (**Figure 2a**) analogous to that shown for laser-induced hydrothermal growth of metal oxides such as ZnO[14]. As shown in the COMSOL thermal simulation in **Figure 2b,** a relatively low laser input energy (1 mW) can produce a temperature rise (~80 C) that is localized to the beam position (focused here on a 50 nm film of sputtered carbon) and hot enough to locally induce crystallization in the bulk solution[10]. Indeed, following immersion in a precursor solution, crystallites were rapidly generated at the position of the laser spot. By translating the beam in relation to the substrate, perovskite structures could be extended into arbitrary forms (**Figure 2c-e**). Figure 2c and **Supporting Movie 1** shows a time-lapse sequence of the fabrication procedure which provides insight into the initial stages of LDW crystal growth. To mitigate dissolution, these structures were fabricated at near saturation concentration of $CH_3NH_3PbBr_3$ in DMF (~1.7 M). Initial heating and translation of the laser-

induced temperature gradient results in the formation of a polycrystalline 'line' comprised of seeds that are randomly orientated, of which a few are ejected (due to convection) into solution. This process appears to preferentially capture platelet (cuboid) seeds which is likely a consequence of the higher surface area contact and adhesion versus seeds not initially oriented to the substrate. Pausing the beam movement results in further growth/coarsening of the seeds into larger crystals, and additionally, as shown in **Figure 2d-2e**, the seeded $CH_3NH_3PbBr_3$ shapes could be further grown following bulk-heating of the substrate (using a broadband light-source).

We measured the photoluminescent (PL) time-resolved decay of a laser patterned, multi-crystalline structure on sputtered carbon and compared the response to a single, mm-sized crystal (SC) grown in bulk solution. **Figure 2f** shows the decay traces indicating similar transport properties of LDW perovskites versus a millimeter-sized single crystal with similar fast (≈ 5 ns, ≈ 3 ns; LDW, SC) and slow (≈ 41 ns, ≈ 30 ns; LDW, SC) decay time constants (individual curve fittings and images of the perovskite structures are shown in **Figure S4**). We note that the relatively fast decay times for $CH_3NH_3PbBr_3$ perovskite observed here is due to quenching effects of the sputtered carbon[15-16] as we observed slower decay (longer lifetime) of the bulk crystal on a non-conducting polystyrene substrate (**Figure 2f,** black trace).

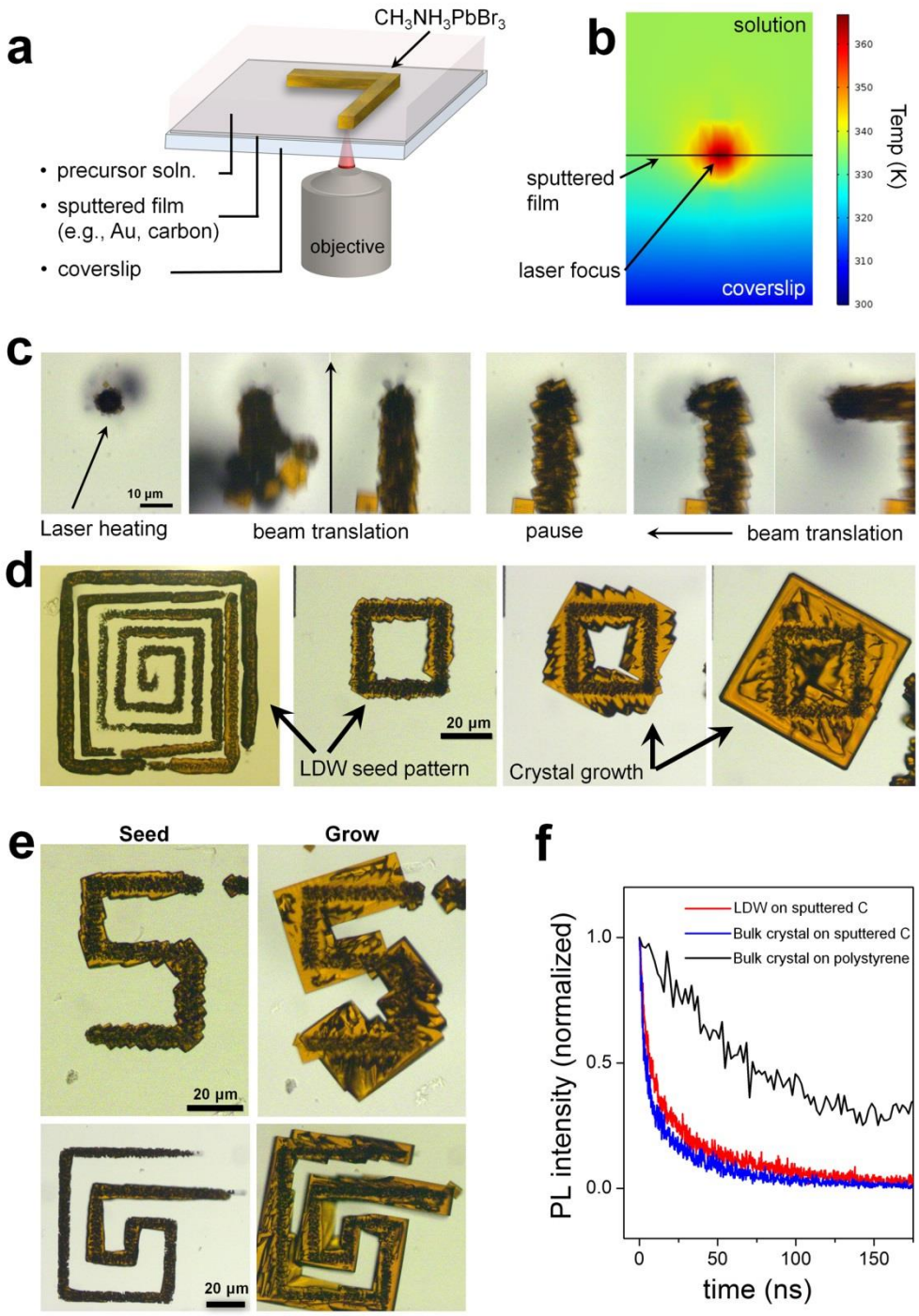

Figure 2. (a) Schematic of LDW to pattern free-form perovskite structures. (b) Thermal simulation (COMSOL) of the temperature gradient induced via 1 mW of focused laser illumination. (c) Time-lapse showing LDW of $CH_3NH_3PbBr_3$ on semi-transparent carbon film (Supporting Movie S1). (d,e) Patterns are seeded with LDW and further grown by heating the substrate using a broadband light source. (f) Photoluminescence decay curves comparing LDW and a bulk solution grown perovskite crystal on the sputtered carbon substrate.

To demonstrate the utility of the LDW perovskite method, we fabricated a $CH_3NH_3PbBr_3$ wire directly onto an interdigitated micro-electrode array to create a micro-photodetection device. **Figure 3a** and **3b** show optical and electron microscope images of the device. As shown in Figure 3b, the perovskite line is composed of large interconnected crystals of $CH_3NH_3PbBr_3$ with average size of 80 μm. We note perovskite films comprised of crystals >20 μm are sometimes termed "single crystalline" perovskites[10, 17] which is an appropriate approximation for this device where the gap between electrodes is 10 μm (single crystals can span the electrodes).

We tested the optical response of the device by measuring current-voltage (I-V) curves to ±100 mV under broad-band illumination. The I-V curves are plotted in **Figure 3c** as a function of irradiance. The curve symmetry about zero reflects the fact that we fabricated a symmetric metal-semiconductor-metal device. The hysteresis in these curves is due to the long relaxation time of the current with respect to the time scale of the current-voltage sweeps. In the inset we show the normalized relaxation of the dark current after abruptly changing the bias from 50mV to 0V. In the inset we show the normalized relaxation of the dark current after abruptly changing the bias from 50mV to 0V (the relaxation time of both charging and discharging is described in **Figure S5** and displays near identical time constants). This slow relaxation has many possible origins (ion migration, trapping and detrapping processes, and others[18]) and warrants more detailed studies[19] for LDW perovskites. However, in devices with direct perovskite-gold contact, the hysteretic behavior has most commonly been attributed to anion migration, leading to built-in electric fields[20-22]. The effect has been observed regardless of anion species within the perovskite (e.g., I or Br) and is independent of perovskite preparation[20]. Our device behaves in accordance with these previous studies and of others who have exploited this behavior for optical/electrical resistive switching memory[21, 23]. Though very simple, the device exhibits a linear response to

irradiance (**Figure 3d**) with strong on/off ratios (dark current levels of ~10^{-12} amps) and demonstrates the ability of the LDW approach to yield functional patterns.

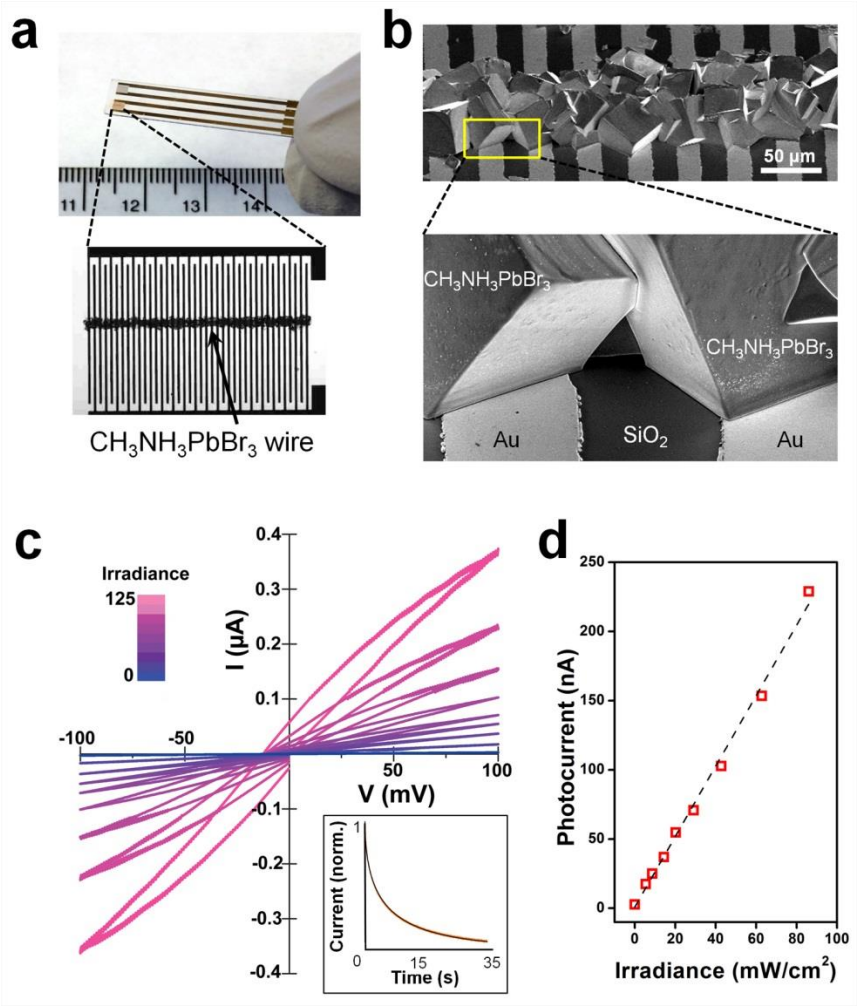

Figure 3. (a) A LDW $MAPbBr_3$ wire drawn onto an Au interdigitated microelectrode (b) SEM of the $CH_3NH_3PbBr_3$ wire. (c) IV traces of the device under varying irradiance by a broadband light source. The inset shows the current relaxation time, fit by a stretched exponential function, observed after changing the bias from 50mV to 0V. (d) Photo-response at +100 mV.

Presently, we have observed that crystallization can be initiated with any photo-thermal transducer (e.g., Au, carbon, Pt, 2D materials[24]), which can be a nanostructure (e.g., dot, cross, etc.), an absorbing thin film or film edge[25]. Similar to the LIHG process, parameters such as laser

spot size, depth of field and thermal conductivity of the transducer are expected to tune the temperature gradient to refine structure formation[14]. We show that LDW can be used to draw perovskite seed structures, which can be grown to large crystals with additional heating. Alternatively the seeds could be dissolved to tune the feature size, e.g., to index structures onto micro-patterned flexible (**Figure 4a, 4b**) and silicon (**Figure 4c, 4d**) substrates. The capability to pattern lead halide perovskites on complex surfaces is enabling for device applications, including lasing[26] and detection platforms using perovskite 'pixels' isolated onto micro-fabricated surfaces. Moreover, fabrication of a well-defined seed layer (e.g., PbX_2[17]) or surface functionalization prior to LDW fabrication and combined with dissolution/recrystallization processes should lead to superior functionality (e.g., high Q-factor lasers[27]).

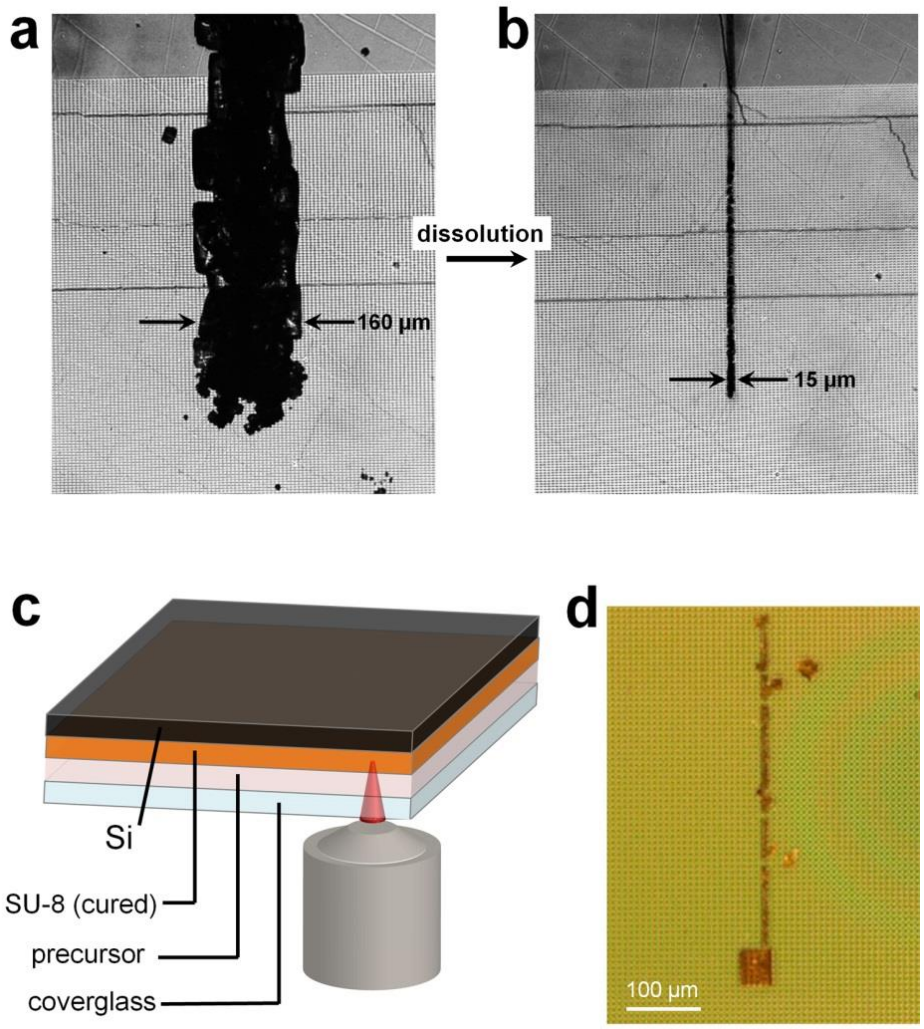

Figure 4. (a) Optical microscope images of a $CH_3NH_3PbBr_3$ line patterned on a polydimethylsiloxane (PDMS) micropatterned substrate coated with 50 nm of sputtered carbon. (b) Slow dissolution of the structures resulted in a uniform 15 µm wide perovskite structures. (c) Schematic showing the fabrication geometry for patterning on a developed and cured SU-8 photoresist microwell pattern on silicon. Optical image of a $CH_3NH_3PbBr_3$ line drawn on the microwell pattern followed by dissolution enables the perovskite structure to index to the microwell pattern (8x8 µm squares, 12 µm deep, spaced with 2 µm thick walls).

We demonstrated LDW of lead halide perovskites from solution to achieve free-form patterning of photoactive materials. The direct-write procedure leverages the inverse temperature solubility of perovskite precursors, enabling site-selective crystallization from solution as directed by laser focus. Overall, this method couples solution-based synthesis of this emerging

class of semiconductors to additive manufacturing and can provide for a straightforward route for the design, iteration and production of perovskite-based devices.

Experimental Methods

$CH_3NH_3PbBr_3$ Precursor Solution: Lead (II) bromide ($PbBr_2$ 99.999%) and N, N-dimethylformamide (DMF, anhydrous, 99.8%) were purchased from Sigma-Aldrich. Methylammonium bromide (MABr) was prepared via stoichiometric neutralization of methylamine with HBr in glacial acetic acid at 0 °C. After stirring for 3 hours, methylammonium bromide was precipitated by the addition of diethyl ether, filtered, washed and dried under vacuum. 1 to 1 solutions of $PbBr_2$/MABr (1/1) were mixed in DMF, dissolved using a bath sonicator, and subsequently filtered using a polytetrafluoroethylene membrane filter (0.2 μm pore size) prior to laser-induced crystallization of methylammonium lead bromide.

Laser Direct Write and Characterization. A Ti:sapphire laser (Tsunami; Spectra Physics) operating at 750 nm was used for all experiments. For deposition of platinum crosses shown in Figure 1 the laser was mode-locked to deliver high frequency (80 MHz) short pulses (60 fs) for multiphoton absorption (for deposition of platinum pads[11]) or continuous wave (CW) mode. The beam was expanded to slightly overfill the back aperture of an oil-immersion objective (Nikon 100× Fluar, 1.3 numerical aperture) situated on an inverted microscope. Laser powers used for these experiments, obtained by attenuating the laser beam using a half-wave plate/polarizing beam-splitter pair, measured between 1-50 mW at the objective. The beam focus was translated in XY using a motorized stage controller to generate simple lines as shown in Figure 2. Seed structures shown in Figure 2 were subsequently grown on the microscope setup using a broadband light source (Halogen Lamp 12V 100W) focused onto the substrate using the microscope condenser. This provided for uniform heating of the substrate (using Kohler illumination) to the field of view.

TEM characterization was carried out in an FEI Tecnai F30 operating at 300 kV using a standard double-tilt holder. The perovskite material was laser-written onto a 300-mesh Cu grid with a lacey carbon support film.

COMSOL Multiphysics 5.2 was used to calculate the expected steady-state temperature rise. A spatially-Gaussian laser pulse (1 mW, 2-μm spot size) at the graphite/glass interface produced an 80 ^{o}C temperature rise in the focus region.

The time-resolved PL (TRPL) measurements were performed using 405 nm wavelength excitation from a frequency-doubled Ti:sapphire laser with ~ 150 fs pulse width and 1 kHz repetition rate. A microscope objective was used to focus the laser source to a spot-size diameter of ~50 μm on the sample surface. The light emitted from the sample was collected through the same objective, focused into an optical fiber, and coupled into a spectrometer attached to a Hamamatsu streak camera with 10 ps temporal resolution.

The perovskite wire shown in Figure 3 was drawn directly onto a prefabricated interdigitated electrode array (NanoSPR LLC). An Agilent B1500A Semiconductor Device

Parameter Analyzer was used to measure the current-voltage and time-dependent characteristics of the interdigitated perovskite device. The device was illuminated in a light-tight enclosure with a high intensity, broadband fiber light source (OSL1, Thorlabs) calibrated using a calibrated reference cell (Oriel Instruments 91150V).

Acknowledgements

This work was supported by the U.S. Department of Energy, Office of Science, Basic Energy Sciences, Materials Sciences and Engineering Division. This work was performed, in part, at the Center for Integrated Nanotechnologies, a U.S. Department of Energy, Office of Basic Energy Sciences user facility. Sandia National Laboratories is a multiprogram laboratory managed and operated by Sandia Corporation, a wholly owned subsidiary of Lockheed Martin Corporation, for the U.S. Department of Energy's National Nuclear Security Administration under Contract No. DE AC04-94AL85000.

Supporting Information Available: Figures S1-S5 and Supporting Movie 1.

References

(1) Kojima, A.; Teshima, K.; Shirai, Y.; Miyasaka, T., Organometal Halide Perovskites as Visible-Light Sensitizers for Photovoltaic Cells. *J. Am. Chem. Soc.* **2009,** *131*, 6050-6051.

(2) Weber, D., CH3NH3PbX3, a Pb(II)-System with Cubic Perovskite Structure. *Z. Naturforsch., B: Chem. Sci.*, **1978**, *3*3, 1443-1444.

(3) Bade, S. G. R.; Li, J.; Shan, X.; Ling, Y.; Tian, Y.; Dilbeck, T.; Besara, T.; Geske, T.; Gao, H.; Ma, B.; et al. Fully Printed Halide Perovskite Light-Emitting Diodes with Silver Nanowire Electrodes. *ACS Nano* **2016,** *10*, 1795-1801.

(4) Shibuya, K.; Koshimizu, M.; Takeoka, Y.; Asai, K., Scintillation Properties of (C6H13NH3)2PbI4: Exciton Luminescence of an Organic/Inorganic Multiple Quantum Well Structure Compound Induced by 2.0 MeV Protons. *Nucl. Instrum. Methods Phys. Res., Sect. B* **2002,** *194*, 207-212.

(5) Tanaka, K.; Takahashi, T.; Ban, T.; Kondo, T.; Uchida, K.; Miura, N., Comparative Study on the Excitons in Lead-Halide-Based Perovskite-Type Crystals $CH_3NH_3PbBr_3$ $CH_3NH_3PbI_3$. *Solid State Commun.* **2003,** *127*, 619-623.

(6) Feng, J.; Yan, X.; Zhang, Y.; Wang, X.; Wu, Y.; Su, B.; Fu, H.; Jiang, L., "Liquid Knife" to Fabricate Patterning Single-Crystalline Perovskite Microplates toward High-Performance Laser Arrays. *Adv. Mater.* **2016**. *28*, 3732-3741.
(7) Cheng, Z. Y.; Wang, Z.; Xing, R. B.; Han, Y. C.; Lin, J., Patterning and Photoluminescent Properties of Perovskite-Type Organic/Inorganic Hybrid Luminescent Films by Soft Lithography. *Chem. Phys. Lett.* **2003,** *376*, 481-486.
(8) Wang, G.; Li, D.; Cheng, H.-C.; Li, Y.; Chen, C.-Y.; Yin, A.; Zhao, Z.; Lin, Z.; Wu, H.; He, Q., Wafer-Scale Growth of Large Arrays of Perovskite Microplate Crystals for Functional Electronics and Optoelectronics. *Sci. Adv.* **2015,** *1*, e1500613.
(9) Niu, L.; Liu, X.; Cong, C.; Wu, C.; Wu, D.; Chang, T. R.; Wang, H.; Zeng, Q.; Zhou, J.; Wang, X., Controlled Synthesis of Organic/Inorganic van der Waals Solid for Tunable Light–Matter Interactions. *Adv. Mater.* **2015,** *27*, 7800-7808.
(10) Saidaminov, M. I.; Abdelhady, A. L.; Murali, B.; Alarousu, E.; Burlakov, V. M.; Peng, W.; Dursun, I.; Wang, L.; He, Y.; Maculan, G.; et al. High-Quality Bulk Hybrid Perovskite Single Crystals within Minutes by Inverse Temperature Crystallization. *Nat. Commun.* **2015,** *6*, 7586.
(11) Zarzar, L. D.; Swartzentruber, B.; Harper, J. C.; Dunphy, D. R.; Brinker, C. J.; Aizenberg, J.; Kaehr, B., Multiphoton Lithography of Nanocrystalline Platinum and Palladium for Site-Specific Catalysis in 3D Microenvironments. *J. Am. Chem. Soc.* **2012,** *134*, 4007-4010.
(12) Poglitsch, A.; Weber, D., Dynamic Disorder in Methylammoniumtrihalogenoplumbates (II) Observed by Millimeter-Wave Spectroscopy. *J. Chem. Phys.* **1987,** *87*, 6373-6378.
(13) Saidaminov, M. I.; Adinolfi, V.; Comin, R.; Abdelhady, A. L.; Peng, W.; Dursun, I.; Yuan, M.; Hoogland, S.; Sargent, E. H.; Bakr, O. M., Planar-Integrated Single-Crystalline Perovskite Photodetectors. *Nat. Commun.* **2015,** *6*, 8724.
(14) Yeo, J.; Hong, S.; Kim, G.; Lee, H.; Suh, Y. D.; Park, I.; Grigoropoulos, C. P.; Ko, S. H., Laser-Induced Hydrothermal Growth of Heterogeneous Metal-Oxide Nanowire on Flexible Substrate by Laser Absorption Layer Design. *ACS Nano* **2015,** *9*, 6059-6068.
(15) Docampo, P.; Ball, J. M.; Darwich, M.; Eperon, G. E.; Snaith, H. J., Efficient Organometal Trihalide Perovskite Planar-Heterojunction Solar Cells on Flexible Polymer Substrates. *Nat. Commun.* **2013,** *4.* 2761.
(16) Chou, S. S.; De, M.; Luo, J.; Rotello, V. M.; Huang, J.; Dravid, V. P., Nanoscale Graphene Oxide (nGO) as Artificial Receptors: Implications for Biomolecular Interactions and Sensing. *J. Am. Chem. Soc.* **2012,** *134*, 16725-16733.
(17) Fu, Y., Meng, F., Rowley, M. B., Thompson, B. J., Shearer, M. J., Ma, D.,Jin, S. Solution Growth of Single Crystal Methylammonium Lead Halide Perovskite Nanostructures for Optoelectronic and Photovoltaic Applications. *J. Am. Chem. Soc.* **2015** *137*, 5810-5818.
(18) Chen, B.; Yang, M.; Priya, S.; Zhu, K., Origin of J–V Hysteresis in Perovskite Solar Cells. *J. Phys. Chem. Lett.* **2016,** *7*, 905-917.
(19) Gottesman, R.; Haltzi, E.; Gouda, L.; Tirosh, S.; Bouhadana, Y.; Zaban, A.; Mosconi, E.; De Angelis, F., Extremely Slow Photoconductivity Response of CH3NH3PbI3 Perovskites Suggesting Structural Changes under Working Conditions. *J. Phys. Chem. Lett.* **2014** 5, 2662-2669.
(20) Stumpp, M.; Ruess, R.; Horn, J.; Tinz, J.; Richter, C.; Schlettwein, D., I–V Hysteresis of Methylammonium Lead Halide Perovskite Films on Microstructured Electrode Arrays:

Dependence on Preparation Route and Voltage Scale. *Phys. Status Solidi A* **2016,** *213*, 38-45.
(21) Xiao, Z.; Yuan, Y.; Shao, Y.; Wang, Q.; Dong, Q.; Bi, C.; Sharma, P.; Gruverman, A.; Huang, J., Giant Switchable Photovoltaic Effect in Organometal Trihalide Perovskite Devices. *Nat. Mater.* **2015,** *14*, 193-198.
(22) Beilsten-Edmands, J.; Eperon, G.; Johnson, R.; Snaith, H.; Radaelli, P., Non-Ferroelectric Nature of the Conductance Hysteresis in CH3NH3PbI3 Perovskite-Based Photovoltaic Devices. *Appl. Phys. Lett.* **2015,** *106*, 173502.
(23) Gu, C.; Lee, J.-S., Flexible Hybrid Organic–Inorganic Perovskite Memory. *ACS Nano* **2016,** *10* (5), 5413-5418.
(24) Chou, S. S.; Kaehr, B.; Kim, J.; Foley, B. M.; De, M.; Hopkins, P. E.; Huang, J.; Brinker, C. J.; Dravid, V. P., Chemically Exfoliated MoS2 as Near-Infrared Photothermal Agents. *Angew. Chem. Int. Ed.* **2013,** *125*, 4254-4258.
(25) Zarzar, L.D.; Swartzentruber, B.S.; Donovan, B.F.; Hopkins, P.E.; Kaehr, B., Using Laser-Induced Thermal Voxels to Pattern Diverse Materials at the Solid-Liquid Interface. *ACS Appl. Mater. Interfaces* **2016,** *8*, 21134–21139.
(26) Wang, K.; Gu, Z.; Liu, S.; Sun, W.; Zhang, N.; Xiao, S.; Song, Q., High-Density and Uniform Lead Halide Perovskite Nanolaser Array on Silicon. *J. Phys. Chem. Lett.* **2016**, 2549-2555.
(27) Zhu, H., Fu, Y., Meng, F., Wu, X., Gong, Z., Ding, Q., Zhu, X. Y. Lead Halide Perovskite Nanowire Lasers with Low Lasing Thresholds and High Quality Factors. *Nat. Mater.*, **2015** *14*, 636-642.